Imperfect Fabry-Perot resonators
Klaassen, T.

CHAPTER 8

Laguerre-Gaussian modes in a bifocal resonator

We investigate the eigenmodes of a cavity, composed of two mirrors, one of which is a bifocal mirror. As the bifocal mirror is rotationally symmetric, it favors a different mode family than traditional stable cavities based upon two monofocal mirrors. A numerical simulation based on an effective index is presented for a better understanding of the optical properties of this system.

8.1 Introduction

In ideal cavities with a rotationally-symmetric quadratic index (or gain) profile, there is considerable degeneracy and the eigenmodes combine to frequency-degenerate classes. Within each of these classes one is free to choose as basis either all Hermite-Gaussian (HG_{mn}) modes with fixed $n + m$ or all Laguerre-Gaussian (LG_{lp}) modes with fixed $2p + |l|$ [12, 74]. Here, m and n indicate the two transverse mode numbers, whereas l and p are the azimuthal and radial mode numbers, respectively. In practical resonators, any small deviation will lead to a preference of one basis over the other. The HG-modes are preferred if the rotational symmetry is broken, and x- and y-axes can be distinguished [12]. The LG-modes are preferred if the rotational symmetry is maintained, but the index profile is nonquadratic [75].

As an interesting example, a Vertical Cavity Surface Emitting Laser (VCSEL) [76,77] can show both cylindrical (LG) and rectangular (HG) modes in one system. The preferred mode-family is now determined by both the physical shape of the cavity and the gain profile in the amplifying medium. The tuning parameter to alter this profile is the injection current; the mode profiles are generally rectangular for low injection currents, but become cylindrical for high injection currents, where thermal lensing and carrier distribution play a more prominent role.

However, in almost any passive resonator the observable eigenmodes are the HG rather than the LG-modes as the rotational symmetry is apparently broken more strongly, by, *e.g.*, astigmatism, than the effective quadratic guiding corresponding to the focussing action of the mirrors [78]. In this Chapter, we will report on a stable cavity in which LG-modes are preferred. Our system is a composite cavity comprising mirrors that are rotationally symmetric, but the height profile consists of two piecewise quadratic parts and is thus nonquadratic as a whole. The system, described in this Chapter, is a first trial in a series of experiments to demonstrate chaos in a open optical resonator; it is equivalent to the geometry discussed by Aiello *et al.* [79] and in Chapter 9 of this thesis.

This Chapter is organized as follows: After introducing the setup, we will report and discuss the measured mode profiles. These profiles will be compared with standard (analytic) LG-modes that exist in paraxial resonators based upon mirrors with a single radius of curvature. A model, based on the concept of an effective index, will be introduced to investigate numerically the effect of the composite height profile. We will finish this Chapter with a concluding discussion.

8.2 Setup

The resonator contains a flat and a composite mirror, as shown in Fig. 8.1. Both substrates have been made out of calcium fluoride (CaF_2) and have been coated in the same run. The measured transmission of the mirrors used in this experiment is $T = 5 \times 10^{-5}$ at a wavelength of $\lambda = 800$ nm. The composite substrate has been diamond-machined. As the composite mirror comprises a convex center (also denoted as "dimple") and a concave annulus, it creates two resonators: a (radially) outer part, which is stable for cavity lengths $L < R = 14$ mm, and a (radially) inner part, which is always unstable. The dimple, in combination with the flat mirror, forms an unstable resonator and acts, in analogy with quantum mechanics, as a rota-

tionally symmetric potential barrier, surrounded by a ditto potential well. This rotational symmetry combined with the nonquadratic (composite) mirror profile imposes LG-eigenmodes.
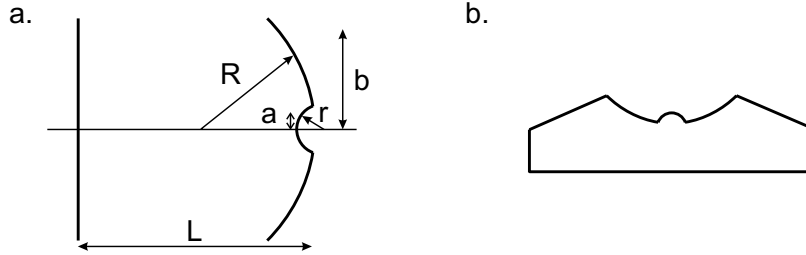

Figure 8.1: *(a) Our cavity configuration, operated at $L = 13.88$ mm, comprises a flat mirror and a bifocal mirror. The dimensions of the bifocal mirror are $R = 14$ mm, $r = -3$ mm, $a = 100$ µm, and $b = 1$ mm. (b) Sketch of the bifocal mirror, where the concave and convex inner part form the mirror. The conical outer part makes the handling of the mirror easier and prevents light to be scattered back into the cavity.*

In order to measure the profiles of the cavity eigenmodes, we use a $f = 10$ cm lens to inject a beam with a waist that is similar to the lowest-order mode of the outer cavity, off-axis under an angle with respect to the optical axis. This is to excite efficiently modes in the stable outer cavity. In order to measure the mode profiles on the bifocal mirror, a lens images the intensity profiles on a CCD-camera with linear intensity response (Apogee Alta U1) behind the cavity. The sub-wavelength control of the cavity length, which is needed to observe individual mode profiles, is obtained with a piezo-element. The cavity is typically operated at cavity lengths $L = 13.5 - 13.9$ mm, close to the instability point $L = R = 14$ mm. The absolute cavity length is calibrated with respect to the 3-fold frequency-degeneracy point ($L = 10.50$ mm). Such a frequency-degenerate point is easy to recognize spectrally and helps to pinpoint the cavity length accurately (few µm).

8.3 Experimental results

As discussed above, in ordinary resonators HG-modes are observed due to the almost unavoidable breaking of the rotational symmetry. We have checked this with a cavity identical to that described above, but without the central convex part. For operation under identical conditions this cavity favors indeed HG-modes. In contrast, the resonator of Fig. 8.1 shows a strong preference for the bifocal-mirror LG-modes. The preference for this mode-family originates apparently from the presence of the rotationally symmetric dimple on the composite mirror.

If we tune the cavity length to $L = 13.88$ mm, *i.e.*, close to instability of the outer cavity, we observe individual modes on the bifocal mirror with a clear rotational symmetry (see Fig. 8.2). The angle and position of injection in this experiment are fixed, and the cavity length is only changed within a free spectral range using the piezo-element. For each radial mode number p, ranging from 1 to 7, we observe LG-modes with various l-numbers. Note the intriguing smaller copies of the outer patterns, which will be discussed below.

The mode profiles, as shown in Fig. 8.2, can be resolved individually and are dominantly observed in a whole range of cavity lengths $L = 13.5 - 13.9$ mm close to the instability of the outer cavity. For shorter cavity lengths, *e.g.*, $L = 7.5$ mm, the rotational symmetry is still present in the intensity profiles; at this length, we do, however, no longer observe individual modes, as many modes are excited at the same time. The reason seems to be that for shorter cavity lengths, the number of available modes is much higher than for larger cavity lengths close to instability. This is related to the size of the waist of the fundamental mode on the outer part of the bifocal mirror, which is $w_0 = 177$ μm for $L = 13.8$ mm, but only $w_0 = 62$ μm for $L = 7.5$ mm. This means that the number of modes that fits inside the aperture of the mirror ($2b = 2$ mm in Fig. 8.1) is $(177/62)^2 = 8$ times lower close to instability than for the shorter cavity length.
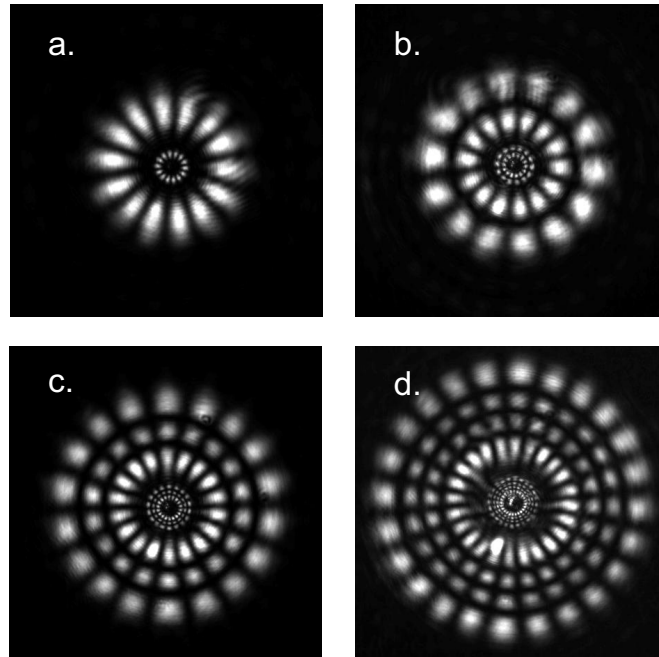

Figure 8.2: *Measured intensity profiles of modes on the bifocal mirror for "fixed cavity length" within a free spectral range. The half-symmetric resonator ($R = 14$ mm) is operated close to instability at a cavity length of $L = 13.88$ mm. The modes shown are (a) $LG_{7,0}$, (b) $LG_{7,1}$, (c) $LG_{9,2}$, and (d) $LG_{12,3}$. The area shown is 1.7×1.7 mm^2 on the bifocal mirror. Note the smaller copy of the intensity profile inside.*

An interesting feature of all experimental mode patterns is that inside the outer mode profile an identical but smaller copy of itself is observed. This inner pattern turns out to be a ghost-image. It results from a combined reflection on the concave side of the imaging lens behind the cavity (typical reflection $R = 1 - 4$ %) and the flat back-mirror of the cavity ($R \approx 100$ %). Imaging with a CCD directly behind the back-mirror of the cavity, *i.e.*, without imaging lens, did not show this copy. The rotationally-averaged intensity profiles shown in

Fig. 8.3 confirm this explanation. At first sight, it might seem strange that the inner image is roughly as intense $(50 - 100 \%)$ as the main image, whereas the expected power reflection is only $1 - 4 \%$. The radius of the inner patterns is, however, about five times smaller than the original patterns, which means that the reflected power is concentrated in a 25 times smaller area. Combined with the intensity as compared to the main image, this corresponds to a power reflection of $2 - 4 \%$, as expected.

8.4 Analytic LG-modes and comparison with experiment

For comparison of the experimental mode profiles with theory, we will now formally introduce the LG-modes [74]. These are solutions of the paraxial wave equation for a stable resonator comprising mirrors with a single radius of curvature (the central dimple will be taken into account in the next Section). The LG-mode profiles in radial coordinates are

$$E_{lp}(r,\phi) = E_0 \rho^l L_{lp}(\rho^2) e^{-\rho^2/2} e^{il\phi} , \qquad (8.1)$$

where l and p are the azimuthal and radial mode numbers, and $\rho \equiv \sqrt{2}r/w_0$ is the dimensionless transverse position. For the fundamental mode we have $E_{00}(\rho) = E_0 \exp(-\rho^2/2) = E_0 \exp(-r^2/w_0^2)$, where w_0 is the waist of the fundamental mode. The Laguerre polynomials L_{lp} are simple expressions, for $p = 0$ to 2 they yield

$$L_{l0}(\rho^2) \quad = \quad 1 , \qquad (8.2)$$
$$L_{l1}(\rho^2) \quad = \quad l + 1 - \rho^2 , \qquad (8.3)$$
$$L_{l2}(\rho^2) \quad = \quad \tfrac{1}{2}(l+1)(l+2) - (l+2)\rho^2 + \tfrac{1}{2}\rho^4 . \qquad (8.4)$$

Higher-order Laguerre polynomials can be found in mathematical handbooks [80].

The $LG_{7,1}$ and $LG_{12,3}$ modes derived from Eq. 8.1 are shown in Fig. 8.3a and c. The images of the calculated modes agree nicely with the measured intensity profiles shown in Fig. 8.2b and d. A more quantitative description and comparison can be made using a rotationally averaged intensity distribution, which is shown in Fig. 8.3b and d for both measured and calculated intensity profiles.

The measured intensity profiles are scaled such that the position of the minimum after the first lobe coincides with the corresponding zero in the calculated intensity profile. This scaling can also be used to pinpoint the waist of the fundamental mode and the exact cavity length. More specifically, the point $\rho = 1$ in the calculated profile corresponds to a radial distance $r = 125$ μm in the measured intensity profile, which results in the waist of the fundamental mode $w_0 = \sqrt{2}r/\rho = 177$ μm. This waist corresponds to a cavity length of $L = 13.8$ mm [12], which is in nice agreement with the cavity length determined previously.

8.5 Numerical calculation of modes in a bifocal resonator

Although the description of the standard LG-modes seems to be sufficient to qualitatively describe the experimental mode profiles, we still want to introduce here a model that can also take into account the presence of the dimple. This allows us to describe the influence of the
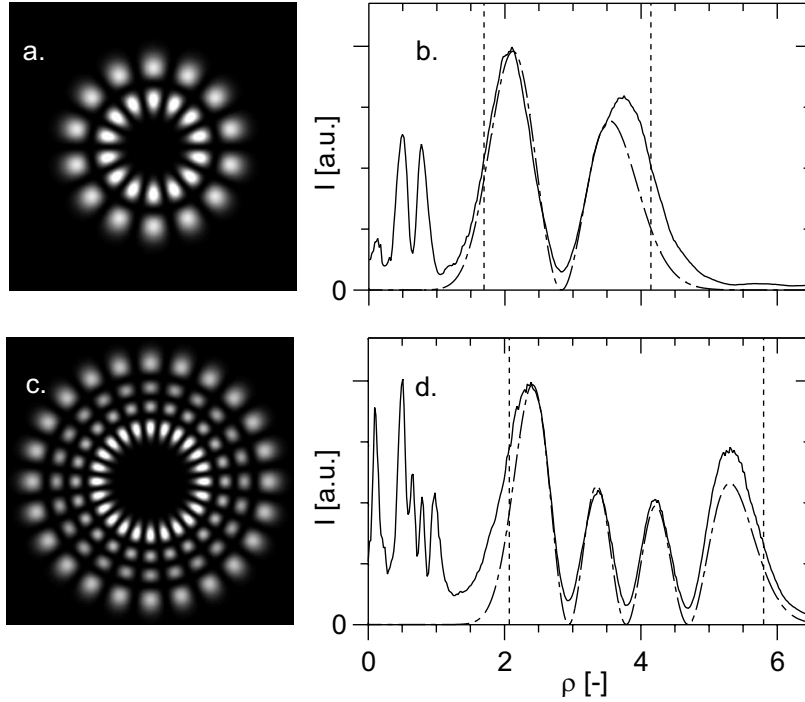
Figure 8.3: *Calculated intensity profiles of the (a) $LG_{7,1}$ and (c) $LG_{12,3}$ modes. The accompanying calculated (dot-dashed lines) and measured (solid lines) rotationally-averaged intensity profiles are shown in (b) and (d). Note the inner copy of the measured intensity profiles. The vertical dotted lines indicate the classical turning points of the modal ray. ρ is the dimensionless transverse position.*

dimple more quantitatively and offers more insight. Additionally, this model allows us to investigate the influence of spherical aberration on the mode profiles; by spherical aberration we mean the deviation of the actual wavefront from a spherical reference wavefront that solely depends on the position of a hit point on the mirror [14].

The transverse modes of the field in the resonator are dictated by the rotational symmetry of the cavity. This restricts the forward propagating electric field to cylindrical coordinates

$$E_{lp}(\rho,\phi,z,t) = \psi_{lp}(\rho,z)e^{i(k_z z - \omega t)}e^{il\phi} \ , \tag{8.5}$$

where $\psi(\rho,z)$ is the slowly varying amplitude of the electric field, k_z the component of the wave vector in the propagation direction, ω the optical frequency, l the angular mode number, and $\rho = \sqrt{2}r/w_0$ is again the dimensionless transverse position.

The so-called effective-index model [81–83] assumes that the (transverse) waveguiding, by either a transverse variation of the electric permittivity ε or, effectively, by a mirror curvature, can be distributed over the length of the cavity and averaged over the axial coordinate. Although this model is strictly valid only if the transverse profile of the field does not change significantly during a full round-trip, we are confident that it will retain its essential features

also beyond this limitation by a simple rescaling in terms of an effective cavity length and an average field.

In the most simple version of the effective index model, the electric permittivity ε is assumed to have the form $\varepsilon = \varepsilon(\rho) = n(\rho)^2$ and consequently the amplitude of the field becomes independent of z and yields $\psi_{lp}(\rho, z) \sim h_{lp}(\rho)$. Application of the effective-index model to a plano-concave resonator means (in more physical terms) that the resonator is reduced to a planar cavity with a built-in radially varying effective index of the form

$$n(\rho) = n_0 \left(1 - \frac{\rho^2 w_0^2}{4RL} \right) , \qquad (8.6)$$

with R the radius of curvature of the mirror. As stated by Hadley [82]; "the effective-index profile is determined by local changes in the Fabry-Perot resonance frequency (for rays that simply travel parallel to, but displaced from, the (z-)symmetry axis)".

Based on Eqs. 8.5 and 8.6, we can rewrite the scalar wave equation for a (slowly varying) amplitude of the field into a Schrödinger-type equation

$$(\nabla_\rho^2 - \rho^2) h_{lp}(\rho) = -2\tilde{\omega} h_{lp}(\rho) , \qquad (8.7)$$

where

$$\nabla_\rho^2 = \frac{\partial^2}{\partial \rho^2} + \frac{1}{\rho} \frac{\partial}{\partial \rho} + \frac{1}{\rho^2} \frac{\partial^2}{\partial \phi^2} , \qquad (8.8)$$

is the rescaled transverse Laplacian, $\tilde{\omega} = \Delta\omega/\omega_G = l + 2p + 1$ a dimensionless eigenfrequency, $\Delta\omega$ is the detuning as compared to an on-axis plane wave and $\omega_G = (c/2L)\theta_0$ is the natural frequency spacing, where θ_0 is the Gouy phase. The term $\frac{1}{\rho^2} \frac{\partial^2}{\partial \phi^2} = -l^2/\rho^2$ in Eq. 8.8 acts as a centrifugal potential, which forces the radial profile $h_{lp}(\rho)$ outwards for higher l.

We solve Eq. 8.7 with the so-called shooting method [84], where the integration proceeds from $\rho = \rho_1 = 0.8$, being the transition from the convex to the concave part of our bifocal mirror, to $\rho = \rho_2$, a position beyond the spatial extent of the mode. We start from $h = 0$ and $\partial h(\rho)/\partial \rho = 1$ and proceed stepwise to the edge using $\partial^2 h(\rho)/\partial \rho^2$ from Eq. 8.7. This iterative process is performed for 2000 consecutive transverse positions ρ. Doing so for various values of $\tilde{\omega}$ for a given l, we find $\tilde{\omega}$ that minimizes the field h at ρ_2 best.

For a more quantitative study of the influence of the dimple on the modes, we have included the dimple (radius $\rho = 0.8$) in our model, replacing ρ^2 in Eq. 8.7 by $R/r\rho^2 = -4\rho^2$, for $\rho < 0.8$. After including the dimple in our model, we can start the integration closer to the center *on* the dimple. We did so for modes with small l-values, like $l = 2$, as these relatively compact modes have the larger spatial extent that overlaps with the dimple and will be affected most. The effect of the dimple is, however, small; the eigenvalue $\tilde{\omega}$ and the position of the maximum change roughly 1 %, and the rising flank of the lobe in the intensity profile shows only a tiny bending point (not shown). The standard analytic LG-modes are thus sufficient to describe our measurements, as the centrifugal term (Eq. 8.8) in Eq. 8.7 still dominates over the potential arising from the dimple structure.

A first remark we want to make is the textbook [85] result that the classical turning points of the mode profiles can be found from Eq. 8.7 by solving $\rho^2 + l^2/\rho^2 - 2\tilde{\omega} = 0$, which results in $\rho^2 = \tilde{\omega} \pm \sqrt{\tilde{\omega}^2 - l^2}$. These points are indicated in Fig. 8.3 for both $LG_{7,1}$ and $LG_{12,3}$, and

coincide with the bending points on the flanks of the first and the last lobes in the intensity profiles.

The second remark is that the model offers the possibility to investigate the effect of aberrations on the mode profiles. As an example, we study spherical aberration, expanding the mirror height profile Δz beyond the quadratic term. Consequently, a fourth order term $-\alpha\rho^4$ has to be added to Eq. 8.7, where α indicates the strength of the aberration and equals $\alpha = 1/(8kR)\sqrt{L/R}$ (see Chapter 4). On second thought, not only the mirror height profile Δz, but also the intra cavity angles, *i.e.*, the transverse momentum of the ray k_z, should be expanded (see Chapter 6). The extra term in Eq. 8.7 is $-\beta\nabla_\rho^4$. The operator formalism of Visser *et al.* [62], discussed in Chapter 6, shows that $\beta = (2R/L)\alpha$ and $\langle\nabla_\rho^4\rangle = \langle\rho^4\rangle$. As a consequence, the second (momentum related) contribution to the spherical aberration is $2R/L$ larger than the one originating from the mirror height profile. The importance of the fourth-order term in the Taylor expansion has been discussed in several other papers that go beyond the paraxial regime [65, 66].

As a quantitative example, we study the strength of spherical aberration for our configuration, *i.e.*, $\alpha = 1.1 \times 10^{-6}$. Taking into account the momentum related contribution, the strength of the spherical aberration becomes $\alpha + \beta = \alpha(1 + 2R/L) \approx 3\alpha = 3.3 \times 10^{-6}$. This number is so small that even far off-axis, close to the edge of the mirror ($\rho = 8$), Eq. 8.7 is still dominated by the quadratic term ρ^2. The influence of spherical aberration on the mode profiles can thus be neglected.

8.6 Concluding discussion

In our system, the profile of the mirror is nonquadratic due to the presence of the central dimple. The dimple is needed to break the quadratic profile of the mirror, but is hardly visible in the mode profile. If we would have destroyed the quadratic profile in any other way, *e.g.*, by drilling a hole in the mirror, we probably would have observed almost identical LG-modes. The latter situation is roughly similar to a potential barrier of infinite height. The approximate mode profiles can be found from the effective-index model starting the integration just outside the dimple.

The discussed preference for a rectangular or cylindrical mode family is not limited to cavities but holds for waveguides [86] as well. To motivate this statement we mention that fibers with an elliptical core prefer a mode family similar to the Hermite-Gaussian (HG) modes in optical resonators [87], whereas fibers with a circular core favor a rotationally symmetric mode family [88]. The stepped (refractive) index of a circular core breaks in fact the quadratic guiding profile so strongly that the mode-profiles are influenced correspondingly and are quite different from the LG-modes. These modes are called LP-modes [89, 90].

In conclusion, we have demonstrated a passive resonator in which LG-modes are preferred, due to the rotational symmetric and nonquadratic profile of the mirror. The intensity profiles on the mirror nicely agree with standard (analytic) LG-modes, showing that the dimple does not yet influence the mode profiles noticeably. This we have checked with an effective-index model, which is also used to demonstrate that the effect of spherical aberration on the mode profiles is still negligible under our operating conditions.